Constraints on a seesaw model leading to quasidegenerate neutrinos and signatures at the LHC

Gulab Bambhaniya,[1,*] Subrata Khan,[1,†] Partha Konar,[1,‡] and Tanmoy Mondal[1,2,§]

[1]*Physical Research Laboratory, Ahmedabad-380009, Gujarat, India*
[2]*Indian Institute of Technology, Gandhinagar-382424, Gujarat, India*

(Received 3 December 2014; revised manuscript received 20 April 2015; published 6 May 2015)

We consider a variant of TeV-scale seesaw models in which three additional heavy right-handed neutrinos are added to the standard model to generate the quasidegenerate light neutrinos. This model is theoretically interesting since it can be fully rebuilt from the experimental data of neutrino oscillations except for an unknown factor in the Dirac-Yukawa coupling. We study the constraints on this coupling coming from metastability of electroweak vacuum. An even stronger bound comes from the lepton flavor violating decays on this model, especially in a heavy neutrino mass scenario which is within the collider's reach. Bestowed with these constrained parameters, we explore the production and discovery potential coming from these heavy neutrinos at the 14 TeV run of the Large Hadron Collider. Signatures with trilepton final state together with backgrounds are considered in a realistic simulation.

DOI: 10.1103/PhysRevD.91.095007 PACS numbers: 12.60.-i, 13.35.Hb, 13.85.Qk, 14.60.St

I. INTRODUCTION

Recent discovery of a neutral scalar [1,2] with a mass around 126 GeV and gradual confirmation of its Standard Model (SM) Higgs-like nature settled the most convincing and self-consisting model of particle physics. However, several experimental observations along with theoretical questions keep the high energy physics community unconvinced that we have yet found our ultimate theory and complete periodic table of particles. So the quest for a new physics beyond the Standard Model is underway both theoretically and experimentally especially with the Large Hadron Collider (LHC) exploring the new horizon of energy and luminosity.

The breakthrough with the Higgs boson also opens up the possibility of exploring new physics by studying the stability of the electroweak vacuum [3,4]. For the SM to be the only valid theory, vacuum should be stable up to Planck scale M_P (1.2×10^{19} GeV) which indicates that the Higgs self-coupling must remain positive through a renormalization group (RG) running up to the Planck scale [5–8]. However, it has been shown [9] that achieving absolute stability within the SM is severely restricted. Yet the self-coupling is not largely negative near the Planck scale which implies that the SM vacuum might be metastable [10,11]. This hypothesis can act as a window to exploring new physics, considering that the SM vacuum should not go to unstable regions [9,12,13]. At least it should remain in the metastable region after inclusion of the effect of new physics.

Seesaw models that lead to light neutrino masses are studied in the context of (meta)stability of the electroweak vacuum [3,4,14–21], lepton flavor violating (LFV) decay [22–24], neutrinoless double beta decay ($0\nu\beta\beta$) (for a recent review, see [25,26]), and new physics signatures of such models at present colliders [27–48]. Seesaw models which consist of extra heavy fields added to the SM predict a hierarchical light neutrino mass spectrum (such as normal hierarchy and inverted hierarchy) as well as a degenerate light neutrino mass spectrum [49–54]. With recent results from Planck data [55], the degenerate mass spectrum becomes severely restricted, although the quasidegenerate (QD) mass spectrum [49–54] is not fully ruled out. It is worthwhile to study QD models in the light of new constraints coming from vacuum (meta)stability and lepton flavor violation (LFV), and also to investigate the possibility of observing signatures of this model at the upcoming 14 TeV LHC.

In this paper we consider a variant of TeV-scale seesaw models consisting of three heavy neutrinos along with the SM, which leads to a quasidegenerate light neutrino mass spectrum. We explore the constraints on the parameters (neutrino Yukawa matrix) coming from the metastability bound. The neutrino Yukawa matrix is constrained significantly from the metastability condition while having weak dependence on the right-handed heavy neutrino mass [17]. The experimental uncertainties from the top quark mass, strong coupling constant, and particularly those from the neutrino data permit a notable window in the constrained value of neutrino Yukawa coupling. The allowed parameter space has been restricted further by combining it with the bound coming from lepton flavor violating (LFV) decay process such as $\mu \to e\gamma$. However, the LFV bound strongly depends on the unknown phases of the Pontecorvo-Maki-Nakagawa-Sakata matrix ($U_{\rm PMNS}$). Considering the best-fit

*gulab@prl.res.in
†subrata@prl.res.in
‡konar@prl.res.in
§tanmoym@prl.res.in

values of oscillation parameters, one would find the bulk of the parameter space (unknown phases), and depending upon the choice of these parameters the LFV constraint can be more restrictive compared to the metastability bound up to ∼TeV.

Once we found the constrained parameters in this model where the neutrino Yukawa matrix is fully reconstructible with the present oscillation data, we study the collider signatures of the heavy neutrinos at 14 TeV LHC. Heavy neutrinos can be produced dominantly through the s-channel production process associated with leptons which subsequently produce a trilepton signal along with missing transverse energy coming from nondetection of the light neutrino. We have considered the leading order production and performed the particle level realistic simulation to estimate this signal using MADGRAPH and PYTHIA. Besides the s-channel process, heavy neutrinos can also be produced through the vector boson fusion (VBF) process, where weak gauge bosons originating from two oppositely moving partons "fuse" to produce these heavy neutrinos. In the VBF production channel, the final new physics signal is accompanied by two forward tagged jets. Since there is no color connection between the two forward tagged jets, the central region is devoid of any color activity. This significantly lowers the background, making weak signals more prominent. These features were exploited not only in the Higgs search (see [56] and references therein), but were also proposed as an avenue to explore new physics [57–60] at the LHC. However, in our case we found that the VBF production cross section of heavy neutrino is too low to provide any conclusive signature in the proposed luminosity.

Organization of the paper goes as follows: Sec. II contains a brief description of the model leading to the quasidegenerate light neutrinos. Vacuum metastability and LFV bounds are discussed in Secs. III and IV, respectively. We also briefly discuss neutrinoless double beta decay in this model in Sec. V. Thereafter we proceed to a collider search strategy by discussing the heavy neutrino production channels at the LHC and heavy neutrino decay in Sec. VI. Detailed simulation, event selection criteria, and expected signal and background results are presented in Sec. VII, followed by discovery potential in Sec. VIII. Finally we summarize and conclude in Sec. IX.

II. THE MODEL

We extend the Standard Model (SM) particle spectra by adding three heavy right-handed neutrinos having mass at the TeV scale. The additional part of the Lagrangian is given by

$$\mathcal{L}_{\text{ext}} = -\tilde{\phi}^{\dagger}\bar{N}_R Y_\nu l_L - \frac{1}{2}\bar{N}_R M N_R^c + \text{H.c.}, \tag{1}$$

where l_L is the left-handed lepton doublet, ϕ is the SM Higgs doublet, and $\tilde{\phi}$ is given by $\tilde{\phi} = i\sigma^2\phi^*$. The right-handed singlet heavy neutrino field is denoted by N_R. $(Y_\nu)_{ji}$ are the elements of the Dirac-Yukawa coupling matrix of dimension (3×3) in the present model with the first (second) index assigned to heavy (light) neutrinos. After spontaneous symmetry breaking, the Higgs field acquires vacuum expectation value v; consequently the light neutrino mass matrix is given by

$$m_\nu = m_D^T M^{-1} m_D, \tag{2}$$

where the Dirac mass term is given by $m_D = Y_\nu v/\sqrt{2}$. Using the parametrization based on Casas and Ibarra [61], texture of the Yukawa coupling matrix Y_ν can be expressed as[1]

$$Y_\nu = \frac{\sqrt{2}}{v}\sqrt{M^d}R\sqrt{m_\nu^d}U_{\text{PMNS}}^{\dagger}, \tag{3}$$

where M^d and m_ν^d are the heavy and light neutrino mass matrices, respectively, in their diagonal basis.[2] U_{PMNS} is the light neutrino mixing matrix, given by

$$U_{\text{PMNS}} = \begin{pmatrix} c_{12}c_{13} & s_{12}c_{13} & s_{13}e^{-i\delta} \\ -c_{23}s_{12} - s_{23}s_{13}c_{12}e^{i\delta} & c_{23}c_{12} - s_{23}s_{13}s_{12}e^{i\delta} & s_{23}c_{13} \\ s_{23}s_{12} - c_{23}s_{13}c_{12}e^{i\delta} & -s_{23}c_{12} - c_{23}s_{13}s_{12}e^{i\delta} & c_{23}c_{13} \end{pmatrix} P, \tag{4}$$

with $c_{mn} = \cos\theta_{mn}$, $s_{mn} = \sin\theta_{mn}$, and δ is the Dirac CP phase. P is the Majorana phase matrix, expressed as $P = \text{diag}(e^{-i\alpha_1/2}, e^{-i\alpha_2/2}, 1)$. For this parametrization of Y_ν, clearly measurable parameters from the low energy neutrino experiments enter through m_ν^d and U_{PMNS}, whereas all unknown parameters are originated from M^d as well as from complex orthogonal matrix R. For simplicity, M^d has been approximated with a single parameter of heavy neutrino mass. Elements of the matrix R are completely arbitrary and can be very large. They eventually elevate the Yukawa couplings [cf. Eq. (3)] to $\mathcal{O}(1)$. On the other hand, owing to the relation $RR^T = I$, these arbitrary elements do not affect the determination of m_ν as in Eq. (2). In other words, the matrix R acts like a fine-tuning parameter which helps to generate sufficiently large Yukawa along with TeV-scale M_R.

[1]For the two-heavy-neutrino case, the parametrization has been studied by Ibarra *et al.* [62].

[2]In the present work we have taken M to be diagonal, which implies that M and M^d are equivalent.

Orthogonality ensures that the matrix R can be written as

$$R = Oe^{iA}, \tag{5}$$

where O and A are real orthogonal[3] and real antisymmetric matrices, respectively. For nearly degenerate light neutrinos one can absorb O in the $U_{\rm PMNS}$ [63]. The general form of the antisymmetric matrix A can be expressed in terms of three unknown parameters

$$A = \begin{pmatrix} 0 & a & b \\ -a & 0 & c \\ -b & -c & 0 \end{pmatrix}, \tag{6}$$

with $a, b, c \in \mathbb{R}^1$. Expanding and rewriting in terms of a new parameter $\omega = \sqrt{a^2 + b^2 + c^2}$ one would obtain

$$e^{iA} = 1 - \frac{\cosh\omega - 1}{\omega^2} A^2 + i \frac{\sinh\omega}{\omega} A. \tag{7}$$

In order to reduce the number of free parameters in our analysis, we choose $a = b = c = \omega/\sqrt{3}$. Now, we are left with a single unknown parameter ω (together with single unknown heavy neutrino mass scale M_R as diagonal entries of matrix M^d) that will be constrained by imposing the bound of metastability of the electroweak vacuum and nonobservation of the LFV decay process. These constraints would in turn be reflected in terms of the norm of the Yukawa coupling matrix which is extremely crucial in production of the heavy neutrinos and essentially determines the discovery potential at the collider. Since Y_ν is a complex square matrix of dimension 3, its magnitude can be best represented in terms of the norm of Y_ν,

$$\mathrm{Tr}[Y_\nu^\dagger Y_\nu] = \frac{2M_R}{v^2} \mathrm{Tr}\left[\sqrt{m_\nu^d} R^\dagger R \sqrt{m_\nu^d}\right], \tag{8}$$

$$= \frac{2M_R}{v^2} m_0 (1 + 2\cosh(2\omega)). \tag{9}$$

One can arrive at the much more compact expression[4] in terms of the parameter ω, as shown in the last equation, assuming an exact degenerate common light neutrino mass scale m_0. For demonstration, contours of constant values of $(\mathrm{Tr}[Y_\nu^\dagger Y_\nu])^{1/2}$ are shown in Fig. 1 with these parameters. For our analysis, the common mass scale for light neutrinos is chosen to be $m_0 \simeq 0.07$ eV, whereas heavy neutrino mass is fixed at 100 GeV. We note that the present allowed light neutrino mass can maximally access the quasidegenerate range, and hence the hierarchical neutrino mass can not be neglected completely. One can parametrize this effect so that the observed neutrino mass hierarchy can be correctly accommodated within this framework of quasidegenerate neutrinos. We classify them as "normal" and "inverted" hierarchies of masses over the common mass scale for light neutrinos. As evident from the figure, for a fixed value of m_0, different values of $(\mathrm{Tr}[Y_\nu^\dagger Y_\nu])^{1/2}$ can be obtained by varying ω accordingly [64]. To present one example, for this particular choice of degenerate light (heavy) neutrino mass of 0.07 eV (100 GeV), the norm $(\mathrm{Tr}[Y_\nu^\dagger Y_\nu])^{1/2} \simeq 0.5$ can be considered for the choice of the parameter[5] $\omega = 13.4$.

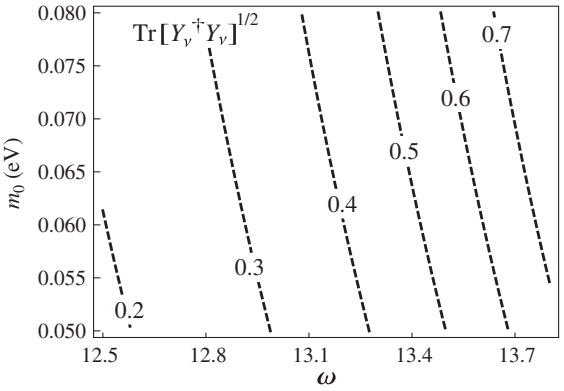

FIG. 1. Parametric plot of $(\mathrm{Tr}[Y_\nu^\dagger Y_\nu])^{1/2}$ with ω and common light neutrino mass scale m_0, and heavy neutrino mass fixed at 100 GeV. The numbers in the plot indicate the corresponding values for the different sets of parameters ω and m_0.

III. METASTABILITY BOUND

The SM potential at tree level is given as

$$\mathcal{V}(\phi) = \lambda(\phi^\dagger\phi)^2 - m^2\phi^\dagger\phi. \tag{10}$$

The physical Higgs mass, in the above convention, is defined as $m_h^2 = 2\lambda v^2$. The renormalization group equation (RGE) of λ can be expressed up to ith loop as

$$\frac{d\lambda}{d\ln\mu} = \sum_i \frac{\beta_\lambda^{(i)}}{(16\pi^2)^i}, \tag{11}$$

where μ is the renormalization scale. The β function for one loop is given as

[3]Satisfying $\det[O] = \det[R]$.

[4]Note that the choice of equal a, b, c parameters does not affect this expression. However, unequal parameters would significantly complicate the LFV calculation in Eq. (22). Also note that if one of the parameters (a, b, or c) is zero, then it is also possible to satisfy the LFV bound, but it is not the case when two parameters are zero.

[5]Note that, for this value of ω, elements of the matrix e^{iA} of Eq. (5) are of $\mathcal{O}(10^6)$ which enhances the Yukawa coupling matrix as in Eq. (3).

$$\beta_\lambda^{(1)} = 24\lambda^2 - \left(\frac{9}{5}g_1^2 + 9g_2^2\right)\lambda + \frac{27}{200}g_1^4 + \frac{9}{20}g_1^2 g_2^2 + \frac{9}{8}g_2^2 + 4T\lambda - 2Y, \quad (12)$$

where

$$T = \mathrm{Tr}[3Y_u{}^\dagger Y_u + 3Y_d{}^\dagger Y_d + Y_l{}^\dagger Y_l + Y_\nu^\dagger Y_\nu], \quad (13)$$

$$Y = \mathrm{Tr}[3(Y_u^\dagger Y_u)^2 + 3(Y_d^\dagger Y_d)^2 + (Y_l^\dagger Y_l)^2 + (Y_\nu^\dagger Y_\nu)^2], \quad (14)$$

and g_i's are the gauge coupling constants. Grand unified theory (GUT) modification for the $U(1)$ gauge coupling has been incorporated. Y_u, Y_d, and Y_l denote the Yukawa coupling matrices for the up-type quark, down-type quark, and charged lepton, respectively. Expectedly, the dominant contribution comes from the top Yukawa (up-type quark) running and the one-loop β function is governed by the following equation:

$$\beta_{Y_u}^{(1)} = Y_u\left[\frac{3}{2}Y_u{}^\dagger Y_u + \frac{3}{2}Y_d{}^\dagger Y_d + T - \left(\frac{17}{20}g_1^2 + \frac{9}{4}g_2^2 + 8g_3^2\right)\right]. \quad (15)$$

Three-loop RGE for Higgs self-coupling (λ), the top Yukawa, and the gauge couplings have been used in the numerical analysis [65–72]. Matching corrections for the top Yukawa have been taken up to three-loop QCD [73], one-loop electroweak [74,75], and $\mathcal{O}(\alpha\alpha_s)$ [7,76], while for Higgs self-coupling, it has been taken up to two loop [9,77]. The Higgs self-coupling also receives additional contribution from the higher order corrections of the effective potential. The loop-corrected[6] effective self-coupling denoted by $\tilde{\lambda}$ is given by [17,78,79]

$$\tilde{\lambda} = \lambda - \frac{1}{32\pi^2}\left[\frac{3}{8}(g_1^2+g_2^2)^2\left(\frac{1}{3} - \ln\frac{(g_1^2+g_2^2)}{4}\right) + 6y_t^4\left(\ln\frac{y_t^2}{2} - 1\right) + \frac{3}{4}g_2^4\left(\frac{1}{3} - \ln\frac{g_2^2}{4}\right) + ([Y_\nu^\dagger Y_\nu]_{ii})^2\left(\ln\frac{[Y_\nu^\dagger Y_\nu]_{ii}}{2} - 1\right) + ([Y_\nu Y_\nu^\dagger]_{jj})^2\left(\ln\frac{[Y_\nu Y_\nu^\dagger]_{jj}}{2} - 1\right)\right] + \frac{Y_t^4}{(16\pi^2)^2}\times \times\left[g_3^2\left\{24\left(\ln\frac{Y_t^2}{2}\right)^2 - 64\ln\frac{Y_t^2}{2} + 72\right\} - \frac{3}{2}Y_t^2\left\{3\left(\ln\frac{Y_t^2}{2}\right)^2 - 16\ln\frac{Y_t^2}{2} + 23 + \frac{\pi^2}{3}\right\}\right], \quad (16)$$

where i, j denote the number of generations of light and heavy neutrinos, respectively. The absolute stability of the electroweak vacuum implies $\tilde{\lambda} \geq 0$ up to Planck scale. However as shown in [9], the absolute stability is highly restrictive. In this light we shall consider metastability; i.e., transition time from a metastable vacuum towards instability should be greater than the age of the Universe. In other words the transition probability through quantum tunneling should be less than unity.

The tunneling probability within the semiclassical approximation is given by (at zero temperature) [10,11,80,81]

$$p = \max_{\mu<\Lambda} V_U \mu^4 \exp\left(-\frac{8\pi^2}{3|\lambda(\mu)|}\right), \quad (17)$$

where Λ is the cutoff scale and V_U is volume of the past light cone, taken as τ^4. Here τ is the age of the Universe taken from Planck data as $\tau = 4.35 \times 10^{17}$ sec [82]. For the vacuum to be metastable, one should have $p < 1$ which can be recast in terms of a lower bound on λ, as given below:

$$|\lambda| < \lambda_{\mathrm{meta}}^{\max} = \frac{8\pi^2}{3}\frac{1}{4\ln(\tau\mu)}. \quad (18)$$

The above equation can be utilized to put an upper bound on $\mathrm{Tr}[Y_\nu^\dagger Y_\nu]$ from the running of λ as a function of the heavy neutrino mass M_R. This has been displayed in Fig. 3 as horizontal slanting lines corresponding to different choices of the top mass and strong coupling. Now, the region below this line is consistent with the metastability bound.

IV. LEPTON FLAVOR VIOLATION BOUND

Lepton flavor violating decay processes get a significant contribution from the heavy neutrino due to its relatively low mass scale compared to the canonical seesaw mechanism. The experimental upper limit on $\mu \to e\gamma$ processes can be translated to an upper bound on $\mathrm{Tr}[Y_\nu^\dagger Y_\nu]$ as a function of M_R. The branching ratio of $\mu \to e\gamma$ [83] is given by

[6]We incorporated two-loop correction due to the SM and one-loop correction due to neutrino Yukawa couplings.

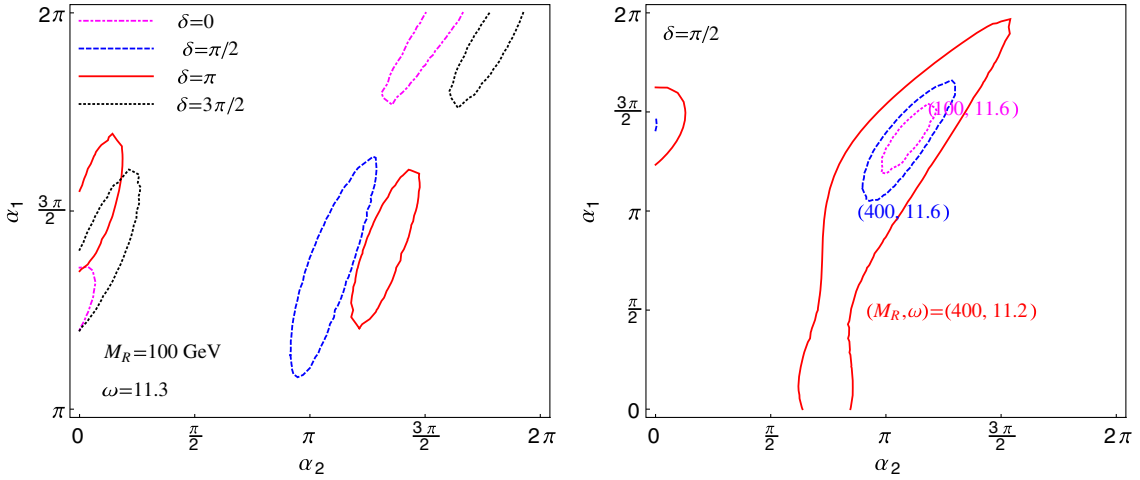

FIG. 2 (color online). Left panel: Contours of allowed lepton flavor violating regions with $\mathrm{Br}(\mu \to e\gamma) = 5.7 \times 10^{-13}$ in the parameter plane of Majorana phases α_1 and α_2 with different values of Dirac CP phase δ. Considering all the neutrino oscillation parameters and mass differences in the global best-fit values, the area within each contour is consistent with the experimental LFV upper bound from the decay rate of $\mu \to e\gamma$. Right panel: Variation of these LFV equality contours for different choices of the heavy neutrino mass M_R and parameter ω considering one example ($\delta = \pi/2$) contour from the left panel. As expected, decreasing the M_R or increasing the ω would make the contour narrower, retaining a smaller window for choices of these unknown parameters.

$$\mathrm{Br}(\mu \to e\gamma) = \frac{3\alpha}{8\pi}\left|\sum_j V_{ej} V^{\dagger}_{j\mu} f(x_j)\right|^2, \tag{19}$$

where dependence of heavy neutrino mass is expressed in terms of dimensionless parameter $x_j = (M^2_{R_j}/m^2_W)$ in a slowly varying function,

$$f(x) = \frac{x(1 - 6x + 3x^2 + 2x^3 - 6x^2 \ln x)}{2(1-x)^4}. \tag{20}$$

In our present case, right-handed neutrinos are degenerate, i.e., $M_{R_j} = M_R$. The light-heavy mixing matrix V is obtained through the diagonalization of the full neutral lepton mass matrix [84]

$$V = m^{\dagger}_D (M^{-1})^* U_R, \tag{21}$$

where U_R is a unitary matrix[7] that diagonalizes M. Using Eqs. (3) and (21) with Eq. (19), one gets

$$\mathrm{Br}(\mu \to e\gamma) = \frac{3\alpha}{8\pi M^2_R}\left[f\left(\frac{M^2_R}{m^2_W}\right)\right]^2 \left|U_{\mathrm{PMNS}} \sqrt{m^d_\nu} R^{\dagger} R \sqrt{m^d_\nu} U^{\dagger}_{\mathrm{PMNS}}\right|^2 \tag{22}$$

and $\mathrm{Tr}[Y^{\dagger}_\nu Y_\nu]$ is given by Eq. (9). From Eqs. (22), (8), and (9) one can see that the angular and phase dependence of the branching ratio comes from the U_{PMNS}, whereas the magnitude of the branching ratio is encoded in $\sqrt{m^d_\nu} R^{\dagger} R \sqrt{m^d_\nu}$, whose modulus is proportional to $\mathrm{Tr}[Y^{\dagger}_\nu Y_\nu]$. The analytical expression of $\mathrm{Br}(\mu \to e\gamma)$ is somewhat lengthy and hence omitted here. Subjected to the present experimental upper bound on the $\mu \to e\gamma$ process [85]

$$\mathrm{Br}(\mu \to e\gamma) \leq 5.7 \times 10^{-13}, \tag{23}$$

one would obtain, numerically, an upper bound on $\mathrm{Tr}[Y^{\dagger}_\nu Y_\nu]$ by inverting Eq. (22).

In a numerical calculation with a very high degree of precision, it is observed that the 3σ uncertainty of the oscillation parameters together with all the phases being varied in the full range [86] would not bound the $\mathrm{Tr}[Y^{\dagger}_\nu Y_\nu]$. Hence, an effective bound on $\mathrm{Tr}[Y^{\dagger}_\nu Y_\nu]$ is coming from vacuum metastability only. To probe this a little further, in Fig. 2 (left panel) we demonstrate the contours of allowed lepton flavor violating regions in the parameter plane of Majorana phases α_1 and α_2 with different values of Dirac CP phase[8] δ. Considering all the neutrino oscillation parameters and mass differences at the global best-fit values (also listed in Table I) [86], the area within each contour is consistent with the experimental LFV upper bound from the decay rate of $\mu \to e\gamma$. Although not conspicuous from the analytic form of multiparameter expression from Eq. (22), one can evaluate that the suitable

[7] U_R is identity matrix in the present scenario as M is diagonal.

[8] In the 3σ range of oscillation parameters, the Dirac CP phase δ is allowed in its full range (0–2π). Also the Majorana phases $\alpha_{1,2}$ are not constrained by oscillation experiments and hence are varied in their full range (0–2π). These three phases are considered here as unknown parameters.

TABLE I. Values of oscillation parameters leading to the upper edge of the yellow shaded region in Fig. 3. We have used global best-fit values of oscillation parameters except the phases.

Parameters	θ_{12}	θ_{23}	θ_{13}	$\Delta^2_{\rm sol}$ (10^{-5} eV^2)	$\Delta^2_{\rm atm}$ (10^{-3} eV^2)	δ	α_1	α_2
Used value	0.19π	0.29π	0.05π	7.62	2.55	1.37π	1.78π	1.67π

and precise choice of δ and α parameters within such contours can indeed evade the bound. In the right panel of Fig. 2 we demonstrate the variation of these LFV equality contours for different choices of the heavy neutrino mass M_R and parameter ω considering once such example ($\delta = \pi/2$) contour from the left panel. As expected, decreasing the M_R or increasing ω would make the contour narrower, retaining a smaller window for choices of these unknown parameters.

From our discussions above, one can clearly choose a parameter for any phenomenological analysis bounded by metastability. However, we took an approach to consider conservative estimates for $\mathrm{Tr}[Y_\nu^\dagger Y_\nu]$ satisfying both LFV and vacuum metastability bounds. To begin with this, we choose a particular set of oscillation parameters such as the global best-fit values of oscillation parameters. Now, if one examines the particular choices of these unknown phases which would be just enough to satisfy the equality of Eq. (23), they are essentially all the points residing over the contours shown in Fig. 2. All the points inside the contours will give $\mathrm{BR}(\mu \to e\gamma) < 5.7 \times 10^{-13}$. Since all the contours are drawn with a fixed ω value, the norm $\mathrm{Tr}[Y_\nu^\dagger Y_\nu]$ will be same over all the contours shown in Fig. 2 (left panel).

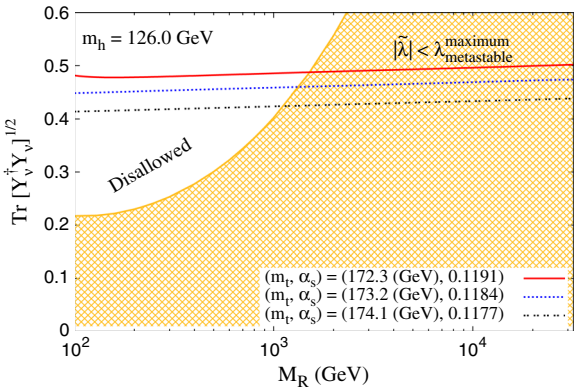

FIG. 3 (color online). Allowed region of the Yukawa norm $\mathrm{Tr}[Y_\nu^\dagger Y_\nu]$ as a function of the heavy neutrino mass M_R by imposing combined constraints coming from metastability of the electroweak vacuum as well as lepton flavor violating decay ($\mu \to e\gamma$). Choice of Higgs mass fixed at $m_h = 126$ GeV. The horizontal slanting lines represent the upper bound on $\mathrm{Tr}[Y_\nu^\dagger Y_\nu]$ consistent with the metastability bound, as in Eq. (18). Three lines are due to three different set of values for top mass and strong coupling [87,88]. The shaded area below the curved line is allowed from the lepton flavor violating constraint as used in Eq. (23). This is after putting global best-fit values of oscillation parameters together with the particular values of unknown phases within their full range as tabulated in Table I. The yellow line corresponds to $\omega = 11.9$ and gives us the best choice for study within the bound of LFV. Hence, the region marked "Disallowed" is ruled out from LFV for such choice of ω.

Dependency of norm $\mathrm{Tr}[Y_\nu^\dagger Y_\nu]$ as a function of heavy neutrino mass is depicted in Fig. 3. The upper bound on the norm is depicted by the golden solid line for $\omega = 11.9$. This gives us the best choice to study within the bound of LFV for this particular value of ω. The yellow shaded area below the curve is allowed[9] from the lepton flavor violating constraint as used in Eq. (23). Hence, the region marked "Disallowed" is strictly ruled out from LFV for such choice of ω.

For our analysis, we have used the value of $\mathrm{Tr}[Y_\nu^\dagger Y_\nu]$ allowed from these constraints which reflects the conservative parameter. To get some notion of related neutrino oscillation parameters, we list them in Table I. They lead to the upper edge of the yellow shaded region as described in Fig. 3. Note that any other choices of ω together with this set of angles and phases will reside in the region.

V. NEUTRINOLESS DOUBLE BETA DECAY

In this section we briefly discuss the contribution of this particular model towards neutrinoless double beta decay ($0\nu\beta\beta$). The general expression of half-life for $0\nu\beta\beta$ in the context of type-I seesaw is given by [89,90]

$$T_{\frac{1}{2}}^{-1} = G\frac{|\mathcal{M}_\nu|^2}{m_e^2}\left|\sum_i (U_{\rm PMNS})_{ei}^2 (m_\nu^d)_i + \sum_j \langle p^2\rangle \frac{V_{ej}^2}{M_{R_j}}\right|^2, \tag{24}$$

where $G = 7.93 \times 10^{-15}$ yr^{-1}, $\mathcal{M}_\nu$ is the nuclear matrix element due to light neutrino exchange, and m_e is the electron mass. $\langle p^2\rangle$ in the second term, which is due to the contributions from heavy singlet neutrinos, is given by [91]

$$\langle p^2\rangle = -m_e m_p \frac{\mathcal{M}_N}{\mathcal{M}_\nu}, \tag{25}$$

which is taken to be $\langle p^2\rangle = -(182\ \mathrm{MeV})^2$ [89]. Here m_p is the proton mass and $\mathcal{M}_N$ is the nuclear matrix element due to heavy neutrino exchange.

[9]This is over the choice of decreasing values of ω parameters.

The first and second terms in Eq. (24) represent contributions from light and heavy neutrinos, respectively, and are thus summed over a corresponding number of light (heavy) neutrinos. Accordingly with the help of Eqs. (3) and (21), the second term can be expressed as

$$\frac{\langle p^2\rangle}{M_R^2}(U_{\rm PMNS}\sqrt{m_\nu^d}R^\dagger R^*\sqrt{m_\nu^d}U_{\rm PMNS}^T)_{ee} = \frac{\langle p^2\rangle}{M_R^2}(U_{\rm PMNS})_{ei}^2(m_\nu^d)_i. \quad (26)$$

Consequently Eq. (24) becomes

$$T_{\frac{1}{2}}^{-1} = G\frac{|\mathcal{M}_\nu|^2}{m_e^2}\left(1+\frac{\langle p^2\rangle}{M_R^2}\right)^2|(U_{\rm PMNS})_{ei}^2(m_\nu^d)_i|^2. \quad (27)$$

One can notice that the contribution on $0\nu\beta\beta$ from heavy neutrinos is extremely tiny, e.g., only 0.001% of the light neutrino contribution can come toward the half-life of $0\nu\beta\beta$ even for a heavy neutrino mass of 100 GeV. This contribution is even suppressed as the mass increased. Although light neutrino contributions to the neutrinoless double beta decay can be sizable and can possibly be explored in future experiments [25], the heavy neutrino contribution in this scenario can be neglected. This outcome is not surprising if one follows from Eq. (26). The large values in the matrix R, which is essential to obtain large Dirac-Yukawa, get canceled. Finally we get very small values of $(VV^T)_{\ell\ell}$ for same sign dilepton (SSDL) production. By the same grounds, collider production of SSDL is suppressed and hence not considered, although the heavy neutrino is of Majorana type. Interestingly, this is a general consequence of Casas-Ibarra parametrization when the heavy neutrinos are degenerate. At the same time large Yukawa makes the opposite sign dilepton cross section [which is proportional to $(VV^\dagger)_{\ell\ell}$] sizable. Large SM background in this channel compelled us to consider for trilepton signal at the LHC. In the next section, we would explore the production of these heavy neutrinos at the collider and discuss the discovery potential for the 14 TeV LHC.

VI. SIGNATURES AT THE LHC

Heavy neutrinos can be produced dominantly in s-channel W-boson exchange at the LHC. We also explored the corresponding VBF production associated with two forward jets. At the leading order calculation, parton level processes producing heavy neutrinos (N) at the mass basis are as follows:

$$q\bar{q}' \to W^{\pm *} \to l^\pm N \quad (s\text{-channel}),$$
$$qq' \to l^\pm N q q'' \quad (\text{VBF}), \quad (28)$$

where q represents suitable partons and associated leptons are $l \equiv (e,\mu,\tau)$. In Fig. 4 (left panel) the total cross section for these processes is shown as a function of heavy neutrino mass after applying the preselection cuts, i.e., $p_{T_l} > 20$ GeV and $|\eta_l| < 2.5$. The solid (dashed) line is showing leading order production cross section through the s-channel (VBF) process. From the figure it is evident that the VBF cross section is insufficient; hence, we shall not discuss this production mechanism afterward and concentrate only on the s-channel process for phenomenological analysis.

For our simulation we consider the maximum allowed value coming from $\mathrm{Tr}[Y_\nu^\dagger Y_\nu]$, satisfying combined LFV and metastability bounds as depicted in Fig. 3, together with neutrino oscillation data within their uncertainties. One can notice that the higher values of Yukawa coupling are

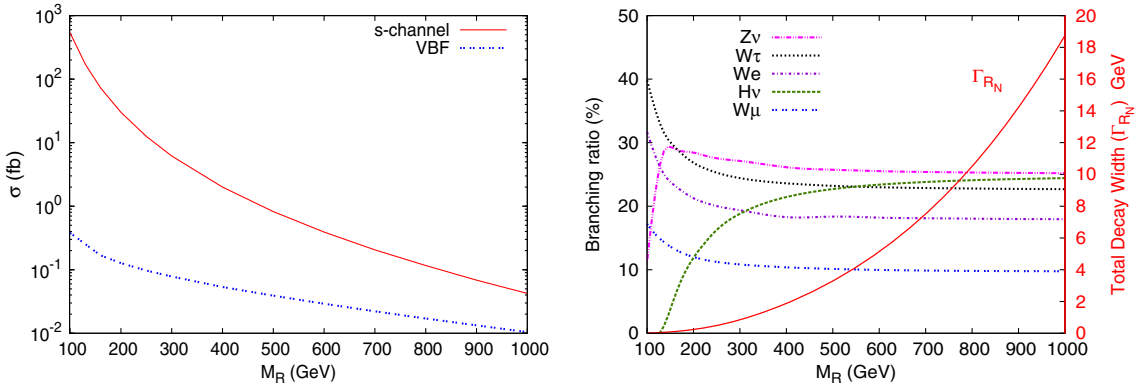

FIG. 4 (color online). Left panel: Total cross section is plotted for leading order s-channel heavy neutrino production (solid line) associated with charged leptons at the 14 TeV LHC. Basic preselection cuts $p_{T\ell} \geq 20$ GeV and $|\eta_\ell| \leq 2.5$ are applied and the choice of parameters is compatible with the neutrino oscillation data constrained with vacuum metastability and LFV. The dotted line shows the corresponding VBF production cross section, where basic VBF cuts were used in addition to the preselection cuts. Right panel: Demonstration of the decay branching ratios of the heavy neutrino in different channels as a function of mass. Total decay width is also shown with a red solid line.

permitted from these constraints once we move toward a higher mass of heavy neutrinos. We have used MADGRAPH5 [92] to simulate the production and decay of heavy neutrinos. Parton distribution function CTEQ6L1 [93] has been used and the factorization scale is set at heavy neutrino mass.

The heavy neutrino can decay into weak gauge bosons ($W^{\pm}, Z$) or the Higgs boson (H) in association with leptons because of mixing between light and heavy neutrinos:

$$N \longrightarrow W^{\pm} l^{\mp} / Z\nu_l / H\nu_l. \tag{29}$$

The branching ratio of N in these channels is shown in Fig. 4 (right panel) with varying heavy neutrino mass M_R. In this plot the red solid line is showing the total decay width (Γ_N) of heavy neutrinos. The figure manifests that the $W\tau$ channel is the dominant decay mode for the low mass region and saturates at ~22% for $M_R \gtrsim 400$ GeV. Both $H\nu$ and $Z\nu$ channels saturate at ~25% in the high mass region, leaving approximately 18% (10%) for the We ($W\mu$) channel.

One can notice that the decay into charged light leptons (e, μ) associated with on-shell W bosons can finally produce a trilepton signal with missing transverse momentum at the LHC. This can be a vital channel searching for QD heavy neutrinos at the LHC. It was shown earlier [48] that the separation of these trilepton signals into separate flavor states can carry useful information on the hierarchical structures of light neutrinos associated with the model. Hence we would also consider flavor-allocated cross sections for signal and the backgrounds.

VII. SIMULATION AND RESULTS

To analyze signals for heavy neutrinos, we have implemented this model in FEYNRULES [94] to generate the Feynman rules compatible for MADGRAPH. Parton-level cross sections were generated using MADGRAPH5 and for showering and hadronization of the les houches [95] event file, PYTHIA6 [96] has been used.

To enhance the signal over background, the selection criteria tabulated in Table II have been implemented. In the top portion of this table, all selection parameters and efficiencies were listed. Cuts entitled with VBF cuts are applied only for the VBF part of the analysis. For details, see Refs. [44,48].

Following from our earlier discussion on heavy neutrino production and decay, we are looking for trilepton production at the LHC,

TABLE II. Selection criteria used in simulation.

Selection criteria	
Lepton identification criteria	$\lvert\eta_\ell\rvert < 2.5$ and $p_{T\ell} > 20$ GeV
Detector efficiency for leptons	Electron efficiency (for e^- and e^+): 0.7 (70%) Muon efficiency (for μ^- and μ^+): 0.9 (90%)
Smearing	Gaussian smearing of electron energy and muon p_T
Jet reconstruction	PYCELL cone algorithm in PYTHIA
Lepton-jet separation	$\Delta R_{lj} \geq 0.4$ (for all jets)
Lepton-lepton separation	$\Delta R_{ll} \geq 0.2$
Lepton-photon separation	$\Delta R_{l\gamma} \geq 0.2$ for all $p_{T\gamma} > 10$ GeV
Hadronic activity (to consider leptons with very little hadronic activity around them)	Hadronic activity for each lepton: $\frac{\sum p_{T_{\text{hadron}}}}{p_{T_l}} \leq 0.2$ ($\equiv$ radius of the cone around the lepton)
Final p_T cuts for leptons	$p_{Tl_1} > 30$ GeV, $p_{Tl_2} > 30$ GeV, and $p_{Tl_3} > 20$ GeV
Missing p_T cut	$\not{p}_T > 30$ GeV
Z-veto[a]	$\lvert m_{\ell_1\ell_2} - M_Z\rvert \geq 6\Gamma_Z$
VBF cuts	
Central jet veto	Any additional jet with $p_T > 20$ GeV, and $\lvert\eta_0\rvert < 2$ events are discarded[b]
Pseudorapidity [97] of charged leptons	$\eta_{j,\min} < \eta_\ell < \eta_{j,\max}$
Cut applied to jets	$p_{Tj_1,j_2} > 20$ GeV $M_{j_1j_2} > 600$ GeV $\eta_{j_1} \cdot \eta_{j_2} < 0$ and $\lvert\eta_{j_1} - \eta_{j_2}\rvert > 4$

[a]Invariant mass for the same flavored and opposite sign lepton pair, $m_{\ell_1\ell_2}$, must be sufficiently away from Z pole.
[b]Pseudorapidity difference between the average of the two forward jets and the additional jet: $\eta_0 = \eta_3 - (\eta_1 + \eta_2)/2$.

TABLE III. Final trilepton with E_T signal cross section in fb produced through s-channel heavy neutrinos for the benchmark mass $M_R = 100$ GeV at the 14 TeV LHC. All event selection cuts were applied (Table II) except the VBF cuts as described in the text. We have also classified total trilepton signals into four different flavor combinations of leptons and presented the expected cross section in each category.

Total signal cross section (fb)	Flavor allocated cross section (fb)			
	eee	$ee\mu$	$e\mu\mu$	$\mu\mu\mu$
2.732	0.318	1.144	1.030	0.2

$$pp \to \ell^{\pm} N \to \ell^{\pm}(W^{\pm}\ell^{\mp}/Z\nu) \to e^{\pm}e^{\pm}e^{\mp}/e^{\pm}\mu^{\pm}e^{\mp}/e^{\pm}\mu^{\pm}\mu^{\mp}/\mu^{\pm}\mu^{\pm}\mu^{\mp} + E_T.$$

The cross section of the final trilepton signal through s-channel heavy neutrino production at the 14 TeV LHC for a benchmark point of $M_R = 100$ GeV is listed in Table III. Here we have incorporated all event selection criteria except the VBF cuts. Total contributions from all the light leptons (e, μ) and the differential contributions from the four flavor combinations are also presented.

All the Standard Model channels that can mimic this trilepton signal with missing E_T are considered for the estimation of SM background. Such simulation events are generated using ALPGEN [98] at the parton level and then passed into PYTHIA for hadronization and showering. We have used the same selection criteria as tabulated in Table II. Inclusive cross section for the $\ell^{\pm}\ell^{\pm}\ell^{\mp}\nu_{\ell}$ final state from the SM is 32.722 fb. Details of an individual channel's contribution toward the SM background can be found in [44,48,99].

VIII. DISCOVERY POTENTIAL

With our understanding on signal strength of producing trileptons from heavy neutrino and possible sources of leading background, it is convenient to present our result in terms of significance which we express as $S/\sqrt{S+B}$, where $S(B) = \mathcal{L}\sigma_{S(B)}$. $\mathcal{L}$ is the integrated luminosity of available data from the experiment and $\sigma_{S(B)}$ is the final cross section of the signal (background) after all event selection cuts and with model parameters of the model satisfying metastability and LFV bound. Figure 5 depicts 3σ (magenta) and 5σ (blue) constant significance contours at the 14 TeV LHC in terms of heavy neutrino mass and integrated luminosity. Horizontal black dotted lines represent integrated luminosity of 300 fb^{-1} and 3000 fb^{-1}. This model can be probed through trilepton signals at the 14 TeV LHC up to $M_R = 160\,(140)$ GeV with 3σ (5σ) significance with integrated luminosity of 300 fb^{-1}, whereas with higher luminosity of 3000 fb^{-1} it can be probed up to ~230(190) GeV. The inset of the figure demonstrates the expected significance of the s-channel trilepton production from heavy neutrino with mass $M_R = 100$ GeV as a function of integrated luminosity. We note that 3σ (5σ) significance can be achieved with integrated luminosity ~43(120) fb^{-1}.

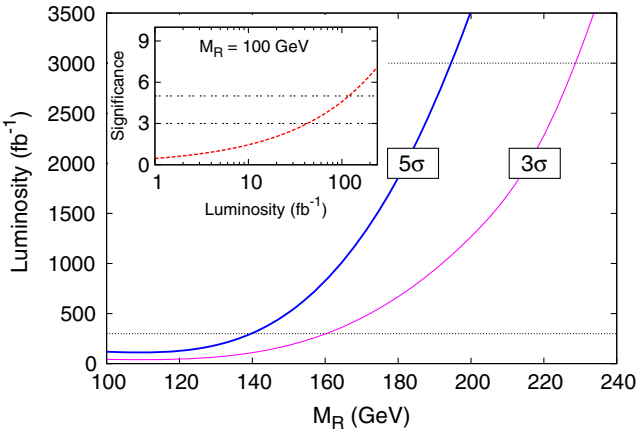

FIG. 5 (color online). Contours of constant 3σ and 5σ significance at the 14 TeV LHC in terms of heavy neutrino mass M_R and integrated luminosity. With 300 fb^{-1} data, the trilepton signal can probe up to $M_R = 160\,(140)$ GeV with 3σ (5σ) significance, whereas with 3000 fb^{-1} luminosity LHC can reach up to 230 (190) GeV. Inset shows variation of significance for the s-channel trilepton production signal and backgrounds with heavy neutrino mass $M_R = 100$ GeV.

IX. CONCLUSION

In this work we have considered a TeV-scale seesaw model that leads to a quasidegenerate light neutrino mass spectrum. The model is fully reconstructible from oscillation parameters apart from an unknown factor parametrized by a constant ω for a common light and heavy neutrino mass scale, m_ν^d and M_R, respectively. We have demonstrated that the norm of Yukawa $\mathrm{Tr}[Y_\nu^\dagger Y_\nu]$ can choose arbitrary magnitude with different choices of ω and the common light neutrino mass scale m_0. Consequently we have obtained bounds on $\mathrm{Tr}[Y_\nu^\dagger Y_\nu]$ from both the consideration of the metastability of the electroweak vacuum and lepton flavor violation. The mass scale of QD light neutrinos is set at $m_0 = 0.07$ eV. Extremely fine-tuned choices of unknown phases evade bounds on $\mathrm{Tr}[Y_\nu^\dagger Y_\nu]$ from LFV. However, the bulk region of parameters allows us a stronger LFV bound than that of the metastability in the low M_R regions. Beyond that mass range, the LFV bound becomes weaker than the metastability bound. The latter remains slowly varying with M_R. However, contribution of the heavy neutrino towards the neutrinoless double beta decay is insignificant in this model compared to the light neutrino contribution.

The constrained model parameters were then used to study the production and decay modes of the heavy neutrino at the LHC. Due to suppressed same sign dilepton

signals in this model, we have studied trileptons associated with a missing E_T signal coming from the s-channel production of the heavy neutrino with realistic selection criteria as well as detailed simulation. However, the similar signal along with two forward tagged jets, coming through the production of heavy neutrinos perceived in vector boson fusion, comes with a much smaller cross section in the present scenario. With a benchmark point of heavy neutrino mass $M_R = 100$ GeV, we have presented the discovery potential of heavy neutrinos, fitted to the model, with 3σ (5σ) significance for integrated luminosity $\sim 42(120)$ fb^{-1} at the 14 TeV LHC. Moreover, this model can be probed for heavy neutrino mass up to 160 (230) GeV for low (high) luminosity options.

ACKNOWLEDGMENTS

We thank M. Ghosh, S. Goswami, and S. Mohanty for useful discussions. P. K. also thanks KIAS group and KIAS workshop for hospitality.

[1] S. Chatrchyan *et al.* (CMS Collaboration), Phys. Lett. B **716**, 30 (2012).
[2] G. Aad *et al.* (ATLAS Collaboration), Phys. Lett. B **716**, 1 (2012).
[3] J. Casas, V. Di Clemente, A. Ibarra, and M. Quiros, Phys. Rev. D **62**, 053005 (2000).
[4] I. Gogoladze, N. Okada, and Q. Shafi, Phys. Lett. B **668**, 121 (2008).
[5] M. Shaposhnikov and C. Wetterich, Phys. Lett. B **683**, 196 (2010).
[6] M. Holthausen, K. S. Lim, and M. Lindner, J. High Energy Phys. 02 (2012) 037.
[7] F. Bezrukov, M. Y. Kalmykov, B. A. Kniehl, and M. Shaposhnikov, J. High Energy Phys. 10 (2012) 140.
[8] S. Alekhin, A. Djouadi, and S. Moch, Phys. Lett. B **716**, 214 (2012).
[9] G. Degrassi, S. Di Vita, J. Elias-Miro, J. R. Espinosa, G. F. Giudice, G. Isidori, and A. Strumia, J. High Energy Phys. 08 (2012) 098.
[10] G. Isidori, G. Ridolfi, and A. Strumia, Nucl. Phys. **B609**, 387 (2001).
[11] J. Espinosa, G. Giudice, and A. Riotto, J. Cosmol. Astropart. Phys. 05 (2008) 002.
[12] J. Ellis, J. Espinosa, G. Giudice, A. Hoecker, and A. Riotto, Phys. Lett. B **679**, 369 (2009).
[13] J. Elias-Miro, J. R. Espinosa, G. F. Giudice, G. Isidori, A. Riotto, and A. Strumia*et al.*, Phys. Lett. B **709**, 222 (2012).
[14] W. Rodejohann and H. Zhang, J. High Energy Phys. 06 (2012) 022.
[15] J. Chakrabortty, M. Das, and S. Mohanty, Mod. Phys. Lett. A **28**, 1350032 (2013).
[16] C.-S. Chen and Y. Tang, J. High Energy Phys. 04 (2012) 019.
[17] S. Khan, S. Goswami, and S. Roy, Phys. Rev. D **89**, 073021 (2014).
[18] D. Buttazzo, G. Degrassi, P. P. Giardino, G. F. Giudice, F. Sala, A. Salvio, and A. Strumia, J. High Energy Phys. 12 (2013) 089.
[19] V. Branchina and E. Messina, Phys. Rev. Lett. **111**, 241801 (2013).
[20] V. Branchina, E. Messina, and A. Platania, J. High Energy Phys. 09 (2014) 182.
[21] V. Branchina, E. Messina, and M. Sher, Phys. Rev. D **91**, 013003 (2015).
[22] S. Petcov, W. Rodejohann, T. Shindou, and Y. Takanishi, Nucl. Phys. **B739**, 208 (2006).
[23] D. Dinh, A. Ibarra, E. Molinaro, and S. Petcov, J. High Energy Phys. 08 (2012) 125.
[24] A. Abada, M. E. Krauss, W. Porod, F. Staub, A. Vicente, and C. Weiland, J. High Energy Phys. 11 (2014) 048.
[25] W. Rodejohann, J. Phys. G **39**, 124008 (2012).
[26] S. Bilenky and C. Giunti, Int. J. Mod. Phys. A **30**, 1530001 (2015).
[27] K. Huitu, J. Maalampi, A. Pietila, and M. Raidal, Nucl. Phys. **B487**, 27 (1997).
[28] A. Akeroyd and M. Aoki, Phys. Rev. D **72**, 035011 (2005).
[29] T. Han and B. Zhang, Phys. Rev. Lett. **97**, 171804 (2006).
[30] F. del Aguila, J. Aguilar-Saavedra, and R. Pittau, J. High Energy Phys. 10 (2007) 047.
[31] T. Han, B. Mukhopadhyaya, Z. Si, and K. Wang, Phys. Rev. D **76**, 075013 (2007).
[32] A. Akeroyd, M. Aoki, and H. Sugiyama, Phys. Rev. D **77**, 075010 (2008).
[33] S. Bray, J. S. Lee, and A. Pilaftsis, Nucl. Phys. **B786**, 95 (2007).
[34] P. Fileviez Perez, T. Han, G.-y. Huang, T. Li, and K. Wang, Phys. Rev. D **78**, 015018 (2008).
[35] F. del Aguila and J. Aguilar-Saavedra, Nucl. Phys. **B813**, 22 (2009).
[36] R. Franceschini, T. Hambye, and A. Strumia, Phys. Rev. D **78**, 033002 (2008).
[37] Z.-Z. Xing, Int. J. Mod. Phys. A **24**, 3286 (2009).
[38] A. Atre, T. Han, S. Pascoli, and B. Zhang, J. High Energy Phys. 05 (2009) 030.
[39] A. Melfo, M. Nemevsek, F. Nesti, G. Senjanovic, and Y. Zhang, Phys. Rev. D **85**, 055018 (2012).
[40] M.-C. Chen and J. Huang, Mod. Phys. Lett. A **26**, 1147 (2011).
[41] O. Eboli, J. Gonzalez-Fraile, and M. Gonzalez-Garcia, J. High Energy Phys. 12 (2011) 009.
[42] S. Vanini (2012), https://inspirehep.net/record/1231294.
[43] A. Das and N. Okada, Phys. Rev. D **88**, 113001 (2013).
[44] G. Bambhaniya, J. Chakrabortty, S. Goswami, and P. Konar, Phys. Rev. D **88**, 075006 (2013).

[45] P. S. B. Dev, A. Pilaftsis, and U.-k. Yang, Phys. Rev. Lett. **112**, 081801 (2014).
[46] J. Aguilar-Saavedra, P. Boavida, and F. Joaquim, Phys. Rev. D **88**, 113008 (2013).
[47] A. Das, P. Bhupal Dev, and N. Okada, Phys. Lett. B **735**, 364 (2014).
[48] G. Bambhaniya, S. Goswami, S. Khan, P. Konar, and T. Mondal, Phys. Rev. D **91**, 075007 (2015).
[49] P. Minkowski, Phys. Lett. **67B**, 421 (1977).
[50] T. Yanagida, Conf. Proc. **C7902131**, 95 (1979).
[51] M. Gell-Mann, P. Ramond, and R. Slansky, Conf. Proc. **C790927**, 315 (1979).
[52] S. Glashow, NATO ASI Ser., Ser. B Phys. **59**, 687 (1980).
[53] R. N. Mohapatra and G. Senjanovic, Phys. Rev. Lett. **44**, 912 (1980).
[54] J. Schechter and J. Valle, Phys. Rev. D **22**, 2227 (1980).
[55] P. Ade *et al.* (Planck Collaboration), Astron. Astrophys. **571**, A16 (2014).
[56] D. L. Rainwater, arXiv:hep-ph/9908378.
[57] A. Datta, P. Konar, and B. Mukhopadhyaya, Phys. Rev. D **65**, 055008 (2002).
[58] A. Datta, P. Konar, and B. Mukhopadhyaya, Phys. Rev. Lett. **88**, 181802 (2002).
[59] D. Choudhury, A. Datta, K. Huitu, P. Konar, S. Moretti, and B. Mukhopadhyaya, Phys. Rev. D **68**, 075007 (2003).
[60] G.-C. Cho, K. Hagiwara, J. Kanzaki, T. Plehn, D. Rainwater, and T. Stelzer, Phys. Rev. D **73**, 054002 (2006).
[61] J. Casas and A. Ibarra, Nucl. Phys. **B618**, 171 (2001).
[62] A. Ibarra and G. G. Ross, Phys. Lett. B **591**, 285 (2004).
[63] S. Pascoli, S. Petcov, and C. Yaguna, Phys. Lett. B **564**, 241 (2003).
[64] S. Goswami, S. Khan, and S. Mishra, Int. J. Mod. Phys. A **29**, 1450114 (2014).
[65] M. Einhorn and D. Jones, Phys. Rev. D **46**, 5206 (1992).
[66] M.-x. Luo and Y. Xiao, Phys. Rev. Lett. **90**, 011601 (2003).
[67] M. E. Machacek and M. T. Vaughn, Nucl. Phys. **B222**, 83 (1983).
[68] M. E. Machacek and M. T. Vaughn, Nucl. Phys. **B236**, 221 (1984).
[69] M. E. Machacek and M. T. Vaughn, Nucl. Phys. **B249**, 70 (1985).
[70] S. Antusch, J. Kersten, M. Lindner, and M. Ratz, Phys. Lett. B **538**, 87 (2002).
[71] L. N. Mihaila, J. Salomon, and M. Steinhauser, Phys. Rev. Lett. **108**, 151602 (2012).
[72] K. Chetyrkin and M. Zoller, J. High Energy Phys. 06 (2012) 033.
[73] K. Melnikov and T. v. Ritbergen, Phys. Lett. B **482**, 99 (2000).
[74] R. Hempfling and B. A. Kniehl, Phys. Rev. D **51**, 1386 (1995).
[75] B. Schrempp and M. Wimmer, Prog. Part. Nucl. Phys. **37**, 1 (1996).
[76] F. Jegerlehner and M. Y. Kalmykov, Nucl. Phys. **B676**, 365 (2004).
[77] A. Sirlin and R. Zucchini, Nucl. Phys. **B266**, 389 (1986).
[78] J. Casas, J. Espinosa, and M. Quiros, Phys. Lett. B **342**, 171 (1995).
[79] J. Casas, J. Espinosa, and M. Quiros, Phys. Lett. B **382**, 374 (1996).
[80] S. R. Coleman, Phys. Rev. D **15**, 2929 (1977).
[81] J. Callan, G. Curtis, and S. R. Coleman, Phys. Rev. D **16**, 1762 (1977).
[82] P. Ade *et al.* (Planck Collaboration), Astron. Astrophys. **571**, A1 (2014).
[83] D. Tommasini, G. Barenboim, J. Bernabeu, and C. Jarlskog, Nucl. Phys. **B444**, 451 (1995).
[84] W. Grimus and L. Lavoura, J. High Energy Phys. 11 (2000) 042.
[85] J. Adam *et al.* (MEG Collaboration), Phys. Rev. Lett. **110**, 201801 (2013).
[86] D. Forero, M. Tortola, and J. Valle, Phys. Rev. D **86**, 073012 (2012).
[87] Tevatron Electroweak Working Group, CDF, D0 Collaborations, arXiv:1107.5255.
[88] S. Bethke, Eur. Phys. J. C **64**, 689 (2009).
[89] M. Mitra, G. Senjanovic, and F. Vissani, Nucl. Phys. **B856**, 26 (2012).
[90] J. Chakrabortty, H. Z. Devi, S. Goswami, and S. Patra, J. High Energy Phys. 08 (2012) 008.
[91] V. Tello, M. Nemevsek, F. Nesti, G. Senjanovic, and F. Vissani, Phys. Rev. Lett. **106**, 151801 (2011).
[92] J. Alwall, M. Herquet, F. Maltoni, O. Mattelaer, and T. Stelzer, J. High Energy Phys. 06 (2011) 128.
[93] J. Pumplin, D. Stump, J. Huston, H. Lai, P. M. Nadolsky, and W.-K. Tung, J. High Energy Phys. 07 (2002) 012.
[94] N. D. Christensen and C. Duhr, Comput. Phys. Commun. **180**, 1614 (2009).
[95] J. Alwall, A. Ballestrero, P. Bartalini, S. Belov, E. Boos *et al.*, Comput. Phys. Commun. **176**, 300 (2007).
[96] T. Sjostrand, S. Mrenna, and P. Z. Skands, J. High Energy Phys. 05 (2006) 026.
[97] G. Bozzi, B. Jager, C. Oleari, and D. Zeppenfeld, Phys. Rev. D **75**, 073004 (2007).
[98] M. L. Mangano, M. Moretti, F. Piccinini, R. Pittau, and A. D. Polosa, J. High Energy Phys. 07 (2003) 001.
[99] G. Bambhaniya, J. Chakrabortty, J. Gluza, M. Kordiaczynska, and R. Szafron, J. High Energy Phys. 05 (2014) 033.